Meccanica (2018) 53:1105–1114
https://doi.org/10.1007/s11012-017-0787-x

Spider weight dragging and lifting mechanics

Nicola M. Pugno

Received: 7 September 2017 / Accepted: 26 October 2017 / Published online: 6 November 2017

Abstract Spiders can produce different types of silk for a variety of purposes, such as making webs for capturing prey, sheets for wrapping, anchorages for connecting threads to surfaces, nest-building, cocoons for protecting eggs, dragline for safe locomotion and ballooning. An additional mechanism, only recently video recorded and never discussed in the literature, is spider weight lifting. Of conceptual importance comparable to that of other key spider mechanisms such as ballooning, spider weight lifting—preceded by a dragging phase for vertical alignment of weight and anchorage—is studied here. It emerges as a smart technique, allowing a single spider to lift weights in principle of any entity just using a tiny pre-stress of the silk. Such a pre-stress already occurs naturally with the weight of the spider itself when it is suspended from a thread. Large deformations, high ultimate strain, nonlinear stiffening, re-tensioning of the silk fibers and extra height of the anchoring points are all characteristics of empirical spider silk and of this lifting technique. It will be demonstrated that they all help to increase the efficiency of the mechanism. Toy experiments inspired by the spider lifting are finally proposed and compared with the theory.

Keywords Spider · Silk · Lifting · Dragging

N. M. Pugno (✉)
Laboratory of Bio-Inspired and Graphene Nanomechanics, Department of Civil, Environmental and Mechanical Engineering, University of Trento, Trento, Italy
e-mail: nicola.pugno@unitn.it

N. M. Pugno
School of Engineering and Materials Science, Queen Mary University of London, Mile End Road, London, UK

N. M. Pugno
Ket Lab, Edoardo Amaldi Foundation, Italian Space Agency, Via del Politecnico snc, Rome 00133, Italy

1 Introduction

The aim of this work is to investigate an additional spider ability, only recently recorded and never discussed in the literature, this is the weights lifting. In the spider lifting mechanism the silk constitutive law, in particular the material stiffening and high ultimate strain, is key to the functionality of the technique. Also re-tensioning of the silk fibers and an extra height anchoring point are shown to increase the efficiency of the mechanism. The unique recorded video of a spider *Olios coenobitus* lifting the empty shell of a snail is available online (https://www.youtube.com/watch?v=-n8nbL2ZBBU): in the first phase, dragging of the shell on the bottom surface is observed for vertically aligning it with the anchorage point, Fig. 1; in the second phase, shell lifting takes place, Fig. 2. Note that other spiders, such as *Phonognatha graefeii,* are able to lift large leaves into their webs to build a retreat, but this happens in several

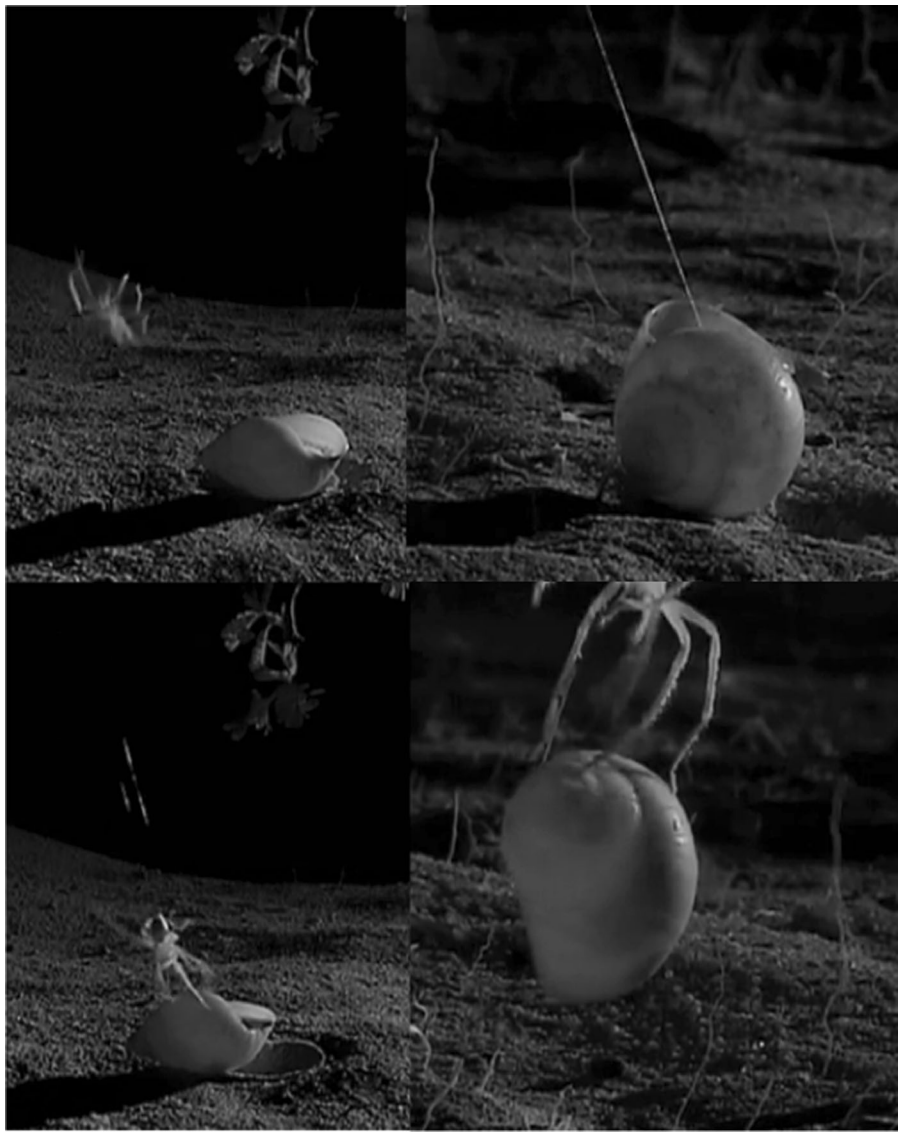

Fig. 1 First phase of the spider weight lifting: n_0 silk fibers with given pre-stresses are attached to the shell; after these n_0 cycles the weight starts to move on the surface towards the projection point on it of the anchorage; additional n_1 fibers are then attached for realizing a second movement, and so on. Simultaneous operations, such as re-tensioning (or even cutting) of the previous fibers, can be done. After a total number of fibers/cycles N_I, of the order of the ratio between the weight of the body to be lifted and the spider weight, the first phase of dragging is terminated: the shell is vertically aligned with the anchorage, touching lightly the substrate, being fully suspended by the silk stressed fibers. In the specific observation $N_I \cong 3$

days and not minutes as observed in this case and type of mechanism. We are investigating the ability of other types of spiders, even more efficient than *Olios coenobitus,* to make direct observations in the lab (work in progress). In this paper the mechanics of the spider's weight dragging and lifting is elucidated. Large deformations, high ultimate strain and nonlinear stiffening seem to be key for this mechanism and are all characteristics of the empirical silk.

In particular, the properties of spider silks and webs [1], ranging from the protein sequence [2] of the silk to the geometry of the web [3], have intrigued scientists as highly adapted materials and structures [4, 5], with exemplary mechanical properties and robustness [6–11]. The spider (genome) is a prime

Fig. 2 Second phase of the spider weight lifting: N_{II} new fibers with given pre-stresses are attached to the shell (at different positions on it, for better lifting weight stability) and simultaneous operations, such as re-tensioning (and even cutting) of the previous fibers, are done as suggested by the absence of floppy threads; after these N_{II} cycles, the shell is lifted from the bottom surface up to the desired height H (the shell is then used for spider protection, e.g. against desiccation). In the specific observation a $\Delta y \cong$ shell size is reached with about 10 cycles when approaching the final height H

example of Nature's evolutionary success. Its silk can surpass in toughness high energy-absorbing materials such as Kevlar, and can be comparable in strength to steel and in density to water thus providing an extremely light-weight alternative [6, 12, 13, 4]. In particular, major ampullate/dragline silk is very tough (e.g. more than Kevlar) while entirely different silks from different glands (many of which predate dragline silk) are used for eggsacs (tubuliform), attachments (pyriform) and so on, and these have vastly different properties. Moreover, a combination of high tensile strength on par with steel of 1–2 GPa and extensibility up to 60% of maximum strain [13] results in superior toughness, and exceeding performance when normalized by its density, leading to about 200 J/g (twice that of Kevlar). Spiders utilize these unique material properties to construct structures which serve a variety of purposes. Indeed, beyond catching insects as prey, spider silk has evolved to fulfill many functions such as the construction of egg sacks and cocoons [14] or attachment disks [15], making it one of the most versatile known materials [9, 16] leading to interest in either natural [17] or artificial production processes [18]. Interest in understanding these materials and structures [19–21] has led to recent studies at the molecular scale [22] of the silks, as well as to the mechanical characteristics of web-like structures [20, 21, 23]. In particular, spider webs are fascinating examples of natural structural engineering essential for an animal's survival [24, 25]. In parallel, spider architecture including the adhesion of anchorages [26, 27] provides inspiration to structural engineers, while matching the remarkable properties of silk fibers presents a challenge to materials scientists [28]. Structural detail can also change material properties and taking inspiration from spider web junctions it has been possible to produce the toughest fibers yet (up to 1400 J/g) thanks to the insertion of loops and sliding knots for dissipating energy via friction [29–32]. However, from a mechanical perspective, it still remains relatively unknown how silk's distinct material behaviour influences the functionality of the structures. That being said, recent work suggests that considering structures separately from materials is no longer sufficient—material properties govern the structural ones and vice versa, creating heightened functionality through synergistic interactions [33–36]. For example, a spider may vary the properties of a piece of thread depending on its placement in the web [37]. A complete understanding of the silk/structure synergy, therefore, requires the merging of studies on material and structural performance, as recently investigated for spider webs [38] and anchorages [39].

2 General constitutive law, large deformations and "natural" pre-stress

With this aim, let us consider the initial configuration as described in Fig. 3 (top left panel), where thus the initial horizontal and vertical distances between centroid of the weight W and point of anchorage (origin of the reference system) are given by x_0, y_0. We consider a nonlinear elastic (dissipation is here neglected) constitutive law of the silk, stress σ versus strain ε, in the general form $\sigma = g(\varepsilon)$ (other, even more general forms, e.g. including dissipation, could be considered). We consider large deformations of the silk and thus its strain is calculated as $\varepsilon = ln\left(\frac{l'}{l}\right)$, where l' is the final length and l is the initial one. Fibers with imposed pre-stress σ are inserted between weight and anchorage, resulting in the first phase of dragging (Figs. 1 and 3 top right panel), terminating with the vertical alignment of the weight centroid and point of anchorage (Fig. 3 bottom left panel), and in the second phase of lifting (Figs. 2 and 3 bottom right panel) the weight. A plausible estimation of the pre-stress σ is its "natural" value due to the body weight w of the spider when suspended on the silk, i.e., $\sigma = \frac{w}{A}$, with A cross-sectional area of the silk fiber. This would be for example the pre-stress of the first silk fiber used for lifting if its deformed length, due to the spider's weight, is exactly equal to the distance between weight and anchorage. Lower pre-stresses are obviously possible as are larger ones if muscular forces are activated; thus, in general, $\sigma = \beta\frac{w}{A}$, where $\beta > 0$ and "naturally" $\beta \cong 1$.

3 Dragging

As stated, in the first phase the weight W is not lifted but dragged on the bottom surface towards the vertical alignment with the anchorage. Initially, n_0 silk fibers of length l_{00} and pre-stress σ_{00} are inserted between

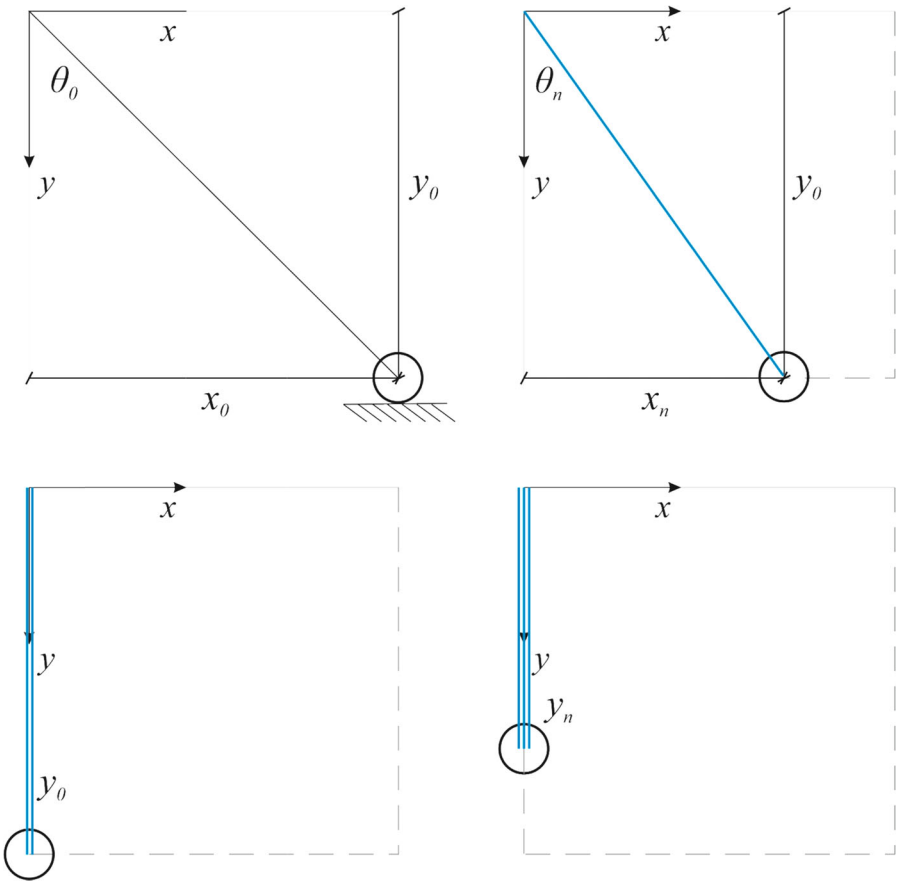

Fig. 3 Spider dragging and lifting phases. Top left panel, initial condition: reference system with origin in the anchorage point and initial coordinates x_0, y_0 of the weight. Top right panel, dragging: pre-stressed silk fibers are attached to the weight and it starts to move horizontally towards the projection on the surface of the anchorage point, thus with coordinates $x_{j\to jl} \to 0, y_0$. Bottom left panel, phase change: end of the first phase and beginning of the second one, at $x_{j=jl} = 0, y_0$; the weight is vertically aligned with the anchorage and touches lightly the substrate, being fully suspended by the silk stressed fibers. Bottom right panel, lifting: the weight is lifted thanks to the insertion of other pre-stressed silk fibers with coordinates $x_j = 0, y_{j\to jll} \to h$, where $h = y_0 - H$ and H is the desired lifting height

weight and anchorage (Figs. 1 and 3 top right panel) causing the first movement of the weight. Note that $l_0 = l_{00}e^{\varepsilon_{00}} = l_{00}e^{g^{-1}(\sigma_{00})} = \frac{x_0}{sin\vartheta_0} = \frac{y_0}{cos\vartheta_0}$, being ϑ_0 the initial angle of the fiber with respect to the vertical direction, from which we could derive l_{00}. The number n_0 can be calculated imposing the horizontal equilibrium of the weight, i.e., $n_0\sigma_{00}sin\vartheta_0 = (W/A - n_0\sigma_{00}cos\vartheta_0)\mu_s$, where μ_s is the static friction coefficient between weight and substrate and as stated $\sigma_{00} = g\left(ln\left(\frac{l_0}{l_{00}}\right)\right)$, $sin\vartheta_0 = \frac{x_0}{l_0}$, $cos\vartheta_0 = \frac{y_0}{l_0}$ and $l_0 = \sqrt{x_0^2 + y_0^2}$. This first step movement stops at a position x_1 that can be deduced, neglecting dynamic effects, by the same equilibrium considering the de-tensioning of the fibers during movement and the dynamic friction coefficient μ_d (between weight and substrate), i.e., $n_0\sigma_{01}sin\vartheta_1 = (W/A - n_0\sigma_{01}cos\vartheta_1)\mu_d$, where σ_{01} is the actual stress in the n_0 fibers at the end of step 1 and is given by $\sigma_{01} = g\left(ln\left(\frac{l_1}{l_{00}}\right)\right)$ as well as $sin\vartheta_1 = \frac{x_1}{l_1}$, $cos\vartheta_1 = \frac{y_0}{l_1}$ and $l_1 = \sqrt{x_1^2 + y_0^2}$. After this first step, a second one can take place inserting new fibers of unstretched length l_{01} and in number n_1 that can be calculated from the new force equilibrium of the weight, i.e., $n_0\sigma_{01}sin\vartheta_1 + n_1\sigma_{11}sin\vartheta_1 = (W/A - n_0\sigma_{01}cos\vartheta_1 - n_1\sigma_{11}cos\vartheta_1)\mu_s$ with $\sigma_{11} = g\left(ln\left(\frac{l_1}{l_{01}}\right)\right)$; it causes the movement of the weight up to a position x_2, that again can be calculated, considering the dynamic friction coefficient and the de-tensioning of the fibers, from the following force equilibrium: $n_0\sigma_{02}sin\vartheta_2 + n_1\sigma_{12}sin\vartheta_2 = (W/A - n_0\sigma_{02}cos\vartheta_2 - n_1\sigma_{12}cos\vartheta_2)\mu_d$ with $\sigma_{02} = g\left(ln\left(\frac{l_2}{l_{00}}\right)\right)$, $\sigma_{12} = g\left(ln\left(\frac{l_2}{l_{01}}\right)\right)$, $sin\vartheta_2 = \frac{x_2}{l_2}$, $cos\vartheta_2 = \frac{y_0}{l_2}$, and $l_2 = \sqrt{x_2^2 + y_0^2}$. In general, at step j, we found the following dragging equations:

$$n_j = \frac{\mu_s W/A - \frac{x_j+\mu_s y_0}{\sqrt{x_j^2+y_0^2}} \sum_{i=0}^{j-1} n_i g\left(ln\left(\frac{\sqrt{x_j^2+y_0^2}}{l_{0i}}\right)\right)}{g\left(ln\left(\frac{\sqrt{x_j^2+y_0^2}}{l_{0j}}\right)\right)\frac{x_j+\mu_s y_0}{\sqrt{x_j^2+y_0^2}}} \tag{1a}$$

$$n_j g\left(ln\left(\frac{\sqrt{x_{j+1}^2+y_0^2}}{l_{0j}}\right)\right)\frac{x_{j+1}+\mu_d y_0}{\sqrt{x_{j+1}^2+y_0^2}} + \frac{x_{j+1}+\mu_d y_0}{\sqrt{x_{j+1}^2+y_0^2}} \sum_{i=0}^{j-1} n_i g\left(ln\left(\frac{\sqrt{x_{j+1}^2+y_0^2}}{l_{0i}}\right)\right) = \mu_d W/A. \tag{1b}$$

Note that for the limiting case of anchorage on the surface ($y_0 = 0$) Eqs. (1) simplify in:

$$n_j = \frac{\mu_s W/A - \sum_{i=0}^{j-1} n_i g\left(ln\left(\frac{x_j}{l_{0i}}\right)\right)}{g\left(ln\left(\frac{x_j}{l_{0j}}\right)\right)} \tag{2a}$$

$$n_j g\left(ln\left(\frac{x_{j+1}}{l_{0j}}\right)\right) + \sum_{i=0}^{j-1} n_i g\left(ln\left(\frac{x_{j+1}}{l_{0i}}\right)\right) = \mu_d W/A. \tag{2b}$$

Different strategies are possible and can strongly affect the dragging and, as we will see, the lifting mechanism too. Let us focus on two strategies of "limiting" complexity. A simple strategy considers unstretched fiber lengths $l_{0i} = l_{00} = const$ at all the steps j (1) whereas a complex one (2) considers the insertion of the new fibers n_j with a pre-stress $\sigma = g(\varepsilon)$ and the simultaneous re-tensioning of the other $\sum_{i=0}^{j-1} n_i$ fibers at the same level of stress or strain, i.e., $l_{0i} = l_{00} = l_{j-1}e^{-\varepsilon}$. Note that after this operation the stress in the fibers is not anymore σ due to de-tensioning, as imposed by the force equilibrium. Also note that fibers removal/cutting can also be considered by correspondingly reducing the numbers n_j. For the simple and complex strategies, Eqs. 1 become respectively:

$$N_j = \sum_{i=0}^{j} n_i = \frac{\mu_s W/A}{g\left(ln\left(\frac{\sqrt{x_j^2+y_0^2}}{l_{00}}\right)\right)\frac{x_j+\mu_s y_0}{\sqrt{x_j^2+y_0^2}}} \tag{3a}$$

$$N_j g\left(ln\left(\frac{\sqrt{x_{j+1}^2+y_0^2}}{l_{00}}\right)\right)\frac{x_{j+1}+\mu_d y_0}{\sqrt{x_{j+1}^2+y_0^2}} = \mu_d W/A \tag{3b}$$

or:

$$N_j = \sum_{i=0}^{j} n_i = \frac{\mu_s W/A}{g\left(ln\left(\frac{\sqrt{x_j^2+y_0^2}}{\sqrt{x_{j-1}^2+y_0^2}}\right)+\varepsilon\right)\frac{x_j+\mu_s y_0}{\sqrt{x_j^2+y_0^2}}} \tag{4a}$$

$$N_j g\left(ln\left(\frac{\sqrt{x_{j+1}^2+y_0^2}}{\sqrt{x_j^2+y_0^2}}\right)+\varepsilon\right)\frac{x_{j+1}+\mu_d y_0}{\sqrt{x_{j+1}^2+y_0^2}} = \mu_d W/A. \tag{4b}$$

Note that from Eq. (3b) we can deduce the minimal value $x_{j+1}^{min} = \sqrt{l_{00}^2 - y_0^2}$ achievable by the simple strategy (1) and thus for having $x_{j+1} = 0$ we must have $l_{00} \leq y_0$; however, an intermediate complexity strategy (3) could be proposed as a series of cycles each of them following the simple strategy (1) with subsequent shorter lengths l_{00}, considered up to a value of $l_{00} = y_0$ for reaching the vertical alignment. The end of the first phase arises when $x_{j+1} = 0$, achievable only for $l_{00} \leq y_0$ in the first strategy (i) and without limitation in the second strategy (2), after the insertion of:

$$N_I = \frac{W}{\sigma A} \tag{5}$$

total number of fibers, where $\sigma = g\left(ln\left(\frac{y_0}{l_{00}}\right)\right)$ (1) or $\sigma = g\left(ln\left(\frac{y_0}{\sqrt{x_{j-1}^2+y_0^2}}\right)+\varepsilon\right) \cong g(\varepsilon)$ (2) respectively.

At the end of this first dragging phase the weight is vertically aligned with the anchorage and fully suspended by the stressed silk fibers and thus the second phase of lifting can start (Figs. 2 and 3 bottom right panel). Let us assume the validity of Eq. (5), thus all the fibers display the same stress at the end of the first phase; this hypothesis is not limiting the generality of the results and could be easily removed by following the presented rational.

4 Lifting

During the second phase, other new silk pre-stressed fibers, with different lengths and thus pre-stresses, are connected one by one between weight and anchorage. After the insertion of j fibers, the vertical force balance of the weight yields the following lifting equation:

$$\frac{W}{A} = N_I\sigma = N_I\sigma' + \sum_{i=1}^{j}\sigma_i = N_I g\left(ln\left(\frac{y_j}{l_{00}}\right)\right) + \sum_{i=1}^{j} g\left(ln\left(\frac{y_j}{l_{i0}}\right)\right) \quad (6)$$

where l_{i0} is the unstretched length of the ith fiber. Note that the stress of the "old" N_I fibers is not anymore the stress σ but is reduced to a value σ' by the detensioning imposed by the insertion of the new j fibers, each of them having a stress σ_i. The two previously considered strategies are also now considered as "limiting" cases, i.e., $l_{i0} = l_{00} = const$ (1) or $l_{i0} = l_{00} = y_{j-1}e^{-\varepsilon}$ (2). For the two cases and remembering that $l_{00} = y_0e^{-\varepsilon} = y_0e^{-g^{-1}(\sigma)}$, we obtain respectively $y_j = y_0e^{g^{-1}\left(\frac{N_I}{j+N_I}\right)-g^{-1}(\sigma)}$ (1) or $y_j = y_{j-1}e^{g^{-1}\left(\frac{N_I}{j+N_I}\right)-g^{-1}(\sigma)}$ (2) and thus in general:

$$y_j = y_0e^{\left(g^{-1}\left(\frac{N_I}{j+N_I}\right)-g^{-1}(\sigma)\right)\eta j},\ N_I = \frac{W}{\beta w}\ \sigma = \beta\frac{w}{A} \quad (7)$$

where for the first (1) strategy the "efficiency" $\eta = \frac{1}{j}$, whereas for the second (2) one, $\eta = 1$; in general, for different strategies different efficiencies are expected as can be calculated with Eq. (6).The total number N_{II} of fibers inserted in the second phase for lifting the weight up to the desired height $H = y_0 - h$ can be calculated from $y_{j=N_{II}} = h$.

5 Efficiency

The efficiency η is more related to the lifting velocity than to the energetic gravitational efficiency η' of the entire process; the latter one can be calculated as:

$$\eta' = \frac{WH}{N_I wH + w\sum_{j=1}^{N_{II}} y_j} = \frac{\beta}{1+\frac{\sum_{j=1}^{N_{II}} y_j}{N_I H}} = \frac{\beta}{1+\frac{N_{II}\langle y_j\rangle}{N_I H}}. \quad (8)$$

Note that the energy cost of the dragging phase alone basically (identically if $\beta = 1$) reaches the theoretical work to be done for lifting the weight to a height H and thus basically all the energy in the lifting phase is "lost"; accordingly, the energetic efficiency of the dragging + lifting mechanism is low.

6 Non linear stiffening (or softening)

To better elucidate the results let us assume the nonlinear constitutive law in traction in the form of $\sigma = g(\varepsilon) = \sigma_u\left(\frac{\varepsilon}{\varepsilon_u}\right)^{\alpha}$, where the subscript u denotes ultimate values, α is the exponent describing the shape of the constitutive law: linear elasticity is described by $\alpha = 1$, where $\frac{\sigma_u}{\varepsilon_u} = E$ is the silk Young's modulus; $\alpha > 1$ describes stiffening behavior, as usually observed in biological materials, such as spider silk; $0 \le \alpha < 1$ describes softening, as usually observed in engineering materials, such as steel. In such a case and since here $\varepsilon > 0$ (fibers work only under traction), Eqs. (6) and (7) become ($y_j = y_0e^{-\left[1-\left(\frac{N_I}{j+N_I}\right)^{\frac{1}{\alpha}}\right]\varepsilon}$ (1) or $y_j = y_{j-1}e^{-\left[1-\left(\frac{N_I}{j+N_I}\right)^{\frac{1}{\alpha}}\right]\varepsilon}$ (2) are derived for the two strategies respectively):

$$N_I\sigma = N_I\frac{\sigma_u}{\varepsilon_u^{\alpha}}ln^{\alpha}\left(\frac{y_j}{l_{00}}\right) + \frac{\sigma_u}{\varepsilon_u^{\alpha}}\sum_{i=1}^{j} ln^{\alpha}\left(\frac{l_j}{l_{i0}}\right) \quad (9a)$$

$$y_j = y_0e^{-\left[1-\left(\frac{N_I}{n+N_I}\right)^{\frac{1}{\alpha}}\right]\varepsilon\eta j},\ N_I = \frac{W}{\beta w},\ \sigma = \beta\frac{w}{A}, \varepsilon = \left(\frac{\sigma}{\sigma_u}\right)^{\frac{1}{\alpha}}\varepsilon_u. \quad (9b)$$

Equation (9b) shows that placing the anchorage well above the height H to be reached by the weight (as it is seen in the real observation) is beneficial for reducing the related number of cycles N_{II}, even if the energetic cost could increase. For the first strategy (1) the minimal distance from the anchorage that can be reached is $h = y_\infty = y_0e^{-\varepsilon} = l_{00}$, however this strategy could be iterated n times —the strategy of middle complexity (3)— to approach the anchoring point at a distance $h = y_\infty = y_0e^{-n\varepsilon}$ and thus $h = y_{n\to\infty} = 0$. For the second strategy (2) $y_{j\to\infty} = y_0e^{-j\varepsilon}$ and again

Fig. 4 Toy experiments inspired by the spider weight lifting. Elastic fibers are realized by a series of elastic bands and attached to a weight (candleholder). Four different experiments with different number of series and parallel elastic bands are reported. Adding/removing and/or disposing in series/parallel these elastic bands result in the weight lifting. Such experiments are compared with the simplest linear predictions of Eq. (10b) in Table 1

Table 1 Toy experimental results and comparison with linearized theory. Here $N_I = 1$, $y_0 = 31$ cm for the 7 elastic bands (three experiments) or 41 cm for the 8 elastic bands (forth experiment), $l_{00} = k \times 1$cm where k is the number of elastic band in a series and 1 cm is the effective unstretched length of a single band, considered here as the free-parameter for taking into account a linearization around a non-zero finite strain (its apparent value appears nearly doubled). Numbers in bold refer to initial conditions

Number of elastic bands in series+in parallel	$y_0 - y_n^{(exp)}$	$y_0 - y_n^{(theo)}$
7	**0.0**	**0.00**
7+6	13.5	13.46
7+6+5	17.0	18.38
7+6+5+4	21.5	21.22
7+6+5+4+3	24.5	23.29
7+6+5+4+3+2	27.0	25.08
7	**0.0**	**0.00**
4	21.0	20.14
4+4	24.0	22.43
4+4+4	24.5	23.57
4+4+4+4	25.0	24.26
7	**0.0**	**0.00**
6+6	16.5	14.71
5+5+5	20.5	20.29
4+4+4+4	25.0	24.26
3+3+3+3+3	27.5	25.94
2+2+2+2+2+2	30.0	27.86
8	**0**	**0**
4+4	32.0	36.00
2+2+2+2	39.5	39.25

$h = y_\infty = 0$, so the situation after j cycles in strategy (2) is similar to that of strategy (3) for $n = j$ cycles of cycles and thus after j^2 cycles. Note that the jumps $\Delta y_j = y_{j-1} - y_j$ are decreasing with j and $\Delta y_\infty = 0$ (and that $\Delta y_1(\alpha \to 1, \varepsilon \to 0) = \frac{y_0 \varepsilon}{N_I}$ for both the two strategies). Equation (9b) also shows that large pre-stress (over ultimate stress ratio), nonlinear stiffening (as observed in spider silk) and ultimate strain (again as observed in spider silk) are all beneficial characteristics for the lifting mechanics.

7 Linearity

In the case of small deformations and linear constitutive law Eqs. (9) become:

$$N_I\sigma = N_I E\frac{y_j - l_{00}}{l_{00}} + E\sum_{i=1}^{j}\left(\frac{y_j - l_{i0}}{l_{i0}}\right) \tag{10a}$$

$$y_j = \frac{(1+\varepsilon)N_I + j}{\frac{N_I}{l_{00}} + \sum_{i=1}^{j} l_{i0}^{-1}}. \tag{10b}$$

For $l_{i0} = const$, $y_j = \frac{(1+\varepsilon)N_I+j}{\frac{N_I}{l_{00}}+\frac{j}{l_{i0}}}$ and accordingly $y_\infty = l_{i0}$ and if, in addition, $l_{i0} = l_{00}$, i.e., the first strategy (1) holds, $y_j = l_{00}\frac{(1+\varepsilon)N_I+j}{N_I+j}$ and thus $y_\infty = l_{00} = \frac{y_0}{1+\varepsilon}$; accordingly, for n iterations and following the middle complexity strategy (3) $y_\infty = \frac{y_0}{(1+\varepsilon)^n}$. For the second strategy (2) $l_{i0} = l_{00} = \frac{y_{j-1}}{1+\varepsilon}$, and thus $y_j = y_{j-1}\frac{(1+\varepsilon)N_I+j}{(N_I+j)(1+\varepsilon)}$ and $y_{j\to\infty} = \frac{y_{j-1}}{1+\varepsilon} = \frac{y_0}{(1+\varepsilon)^j}$. Accordingly in general for linearity (of the constitutive law and for small displacements) $y_{j\to\infty} = \frac{y_0}{(1+\varepsilon)^{\eta j}}$ describes a lifting strategy of a given efficiency.

8 Toy experiments

A simple toy experiment is realized as described in Fig. 4. Only the second phase, i.e. pure lifting, is considered. Elastic fibers are realized by a series and parallel of elastic bands and attached to a weight (candleholder). Adding/removing and/or disposing in series/parallel these elastic bands result in the weight lifting. Four different experiments with different number of series and parallel elastic bands are reported. Experiments are compared with the simplest linear predictions of Eq. (10b) in Table 1, where the strain is computed from $\frac{y_0}{1+\varepsilon} = l_{00}$ with l_{00} considered for a series of elastic bands equal to their number multiplied by the unstretched length of a single band; the latter is considered as the single free-parameter for all the comparison, taking into account a linearization around a non-zero finite strain.

9 Conclusions

In this paper we have elucidated for the first time, to the best of our knowledge, the mechanics of spider weight dragging and lifting. The related mechanisms could be of inspiration for engineering solutions of related problems. We cannot exclude that such phenomena have inspired ancient populations and has thus been applied for dragging and lifting weights before the advent of more advanced and energetically efficient technologies.

Acknowledgements N.M.P. is supported by the European Commission H2020 under the Graphene Flagship Core 1 No. 696656 (WP14 "Polymer composites") and FET Proactive "Neurofibres" Grant No. 732344. N.M.P. has performed the toy experiments with the help of his children Giuseppe Maria, Benedetta and Maria Consolata, warmly acknowledged.

References

1. Foelix RF (1996) Biology of spiders, 2nd edn. Oxford University Press/Georg Thieme Verlag, New York/Stuttgart
2. Lefevre T, Rousseau ME, Pezolet M (2007) Protein secondary structure and orientation in silk as revealed by Raman spectromicroscopy. Biophys J 92(8):2885–2895
3. Vollrath F, Mohren W (1985) Spiral geometry in the garden spider's orb web. Naturwissenschaften 72(12):666–667
4. Vollrath F (2010) Spider silk: evolution and 400 million years of spinning, waiting, snagging, and mating. Nature 466(7304):319
5. Vollrath F, Knight DP (2001) Liquid crystalline spinning of spider silk. Nature 410(6828):541–548
6. Agnarsson I, Kuntner M, Blackledge TA (2010) Bioprospecting finds the toughest biological material: extraordinary silk from a giant riverine orb spider. PLoS ONE 5(9):e11234
7. Du N et al (2006) Design of superior spider silk: from nanostructure to mechanical properties. Biophys J 91(12):4528–4535
8. Omenetto FG, Kaplan DL (2010) New opportunities for an ancient material. Science 329(5991):528–531
9. Shao ZZ, Vollrath F (2002) Materials: surprising strength of silkworm silk. Nature 418(6899):741
10. Liu Y, Shao ZZ, Vollrath F (2005) Relationships between supercontraction and mechanical properties of spider silk. Nat Mater 4(12):901–905
11. Swanson BO et al (2006) Variation in the material properties of spider dragline silk across species. Appl Phys A Mater Sci Process 82(2):213–218
12. Gosline JM et al (1999) The mechanical design of spider silks: from fibroin sequence to mechanical function. J Exp Biol 202(23):3295–3303 **(266)**
13. Swanson BO et al (2009) The evolution of complex biomaterial performance: the case of spider silk. Integr Comp Biol 49(1):21–31
14. Rammensee S et al (2008) Assembly mechanism of recombinant spider silk proteins. Proc Natl Acad Sci USA 105(18):6590–6595

15. Sahni V et al (2012) Cobweb-weaving spiders produce different attachment discs for locomotion and prey capture. Nat Commun 3(1106):1–7
16. Vollrath F et al (1996) Structural organization of spider silk. Proc R Soc Lond B Biol Sci 263(1367):147–151
17. Lazaris A et al (2002) Spider silk fibers spun from soluble recombinant silk produced in mammalian cells. Science 295(5554):472–476
18. Lin S et al (2015) Predictive modelling-based design and experiments for synthesis and spinning of bioinspired silk fibres. Nat Commun 6:6892
19. Alam MS, Wahab MA, Jenkins CH (2007) Mechanics in naturally compliant structures. Mech Mater 39(2):145–160
20. Aoyanagi Y, Okumura K (2010) Simple model for the mechanics of spider webs. Phys Rev Lett 104(3):038102
21. Ko FK, Jovicic J (2004) Modeling of mechanical properties and structural design of spider web. Biomacromol 5(3):780–785
22. Keten S, Buehler MJ (2010) Nanostructure and molecular mechanics of spider dragline silk protein assemblies. J R Soc Interface 7(53):1709–1721
23. Alam MS, Jenkins CH (2005) Damage tolerance in naturally compliant structures. Int J Damage Mech 14(4):365–384
24. Hansell MH (2005) Animinal architecture, 1st edn. Oxford University Press, New York
25. Tarakanova A, Buehler MJ (2012) The role of capture spiral silk properties in the diversification of orb webs. J R Soc Interface 9(77):3240–3248
26. Pugno N (2011) The theory of multiple peeling. Int J Fract 171(2):185–193
27. Varenberg M, Pugno NM, Gorb SN (2010) Spatulate structures in biological fibrillar adhesion. Soft Matter 6(14):3269–3272
28. Bosia F, Buehler MJ, Pugno NM (2010) Hierarchical simulations for the design of supertough nanofibers inspired by spider silk. Phys Rev E 82(5):056103
29. Berardo A, Pantano MF, Pugno N (2016) Slip knots and unfastening topologies enhance toughness without reducing strength of silk fibroin fibres. Interface Focus 6:20150060
30. Bosia F, Lepore E, Alvarez NT, Miller P, Shanov V, Pugno N (2016) Knotted synthetic polymer or carbon nanotube microfibres with enhanced toughness, up to 1400 J/g. Carbon 102:116–125
31. Pantano MF, Berardo A, Pugno N (2016) Tightening slip knots in raw and degummed silk to increase toughness without losing strength. Sci Rep 6:18222
32. Pugno N (2014) The "Egg of Columbus" for making the world's toughest fibres. PLoS ONE 9(4):e93079
33. Cranford SW, Buehler MJ (2012) Biomateriomics, 1st edn. Springer, New York
34. Agnarsson I, Blackledge TA (2009) Can a spider web be too sticky? Tensile mechanics constrains the evolution of capture spiral stickiness in orb-weaving spiders. J Zool 278(2):134–140
35. Opell BD, Bond JE (2001) Changes in the mechanical properties of capture threads and the evolution of modern orb-weaving spiders. Evol Ecol Res 3(5):567–581
36. Sensenig A, Agnarsson I, Blackledge TA (2010) Behavioural and biomaterial coevolution in spider orb webs. J Evol Biol 23(9):1839–1856
37. Boutry C, Blackledge TA (2009) Biomechanical variation of silk links spinning plasticity to spider web function. Zoology 112(6):451–460
38. Cranford SW et al (2012) Nonlinear material behaviour of spider silk yields robust webs. Nature 482(7383):72–76
39. Pugno NM, Cranford S, Buehler MJ (2013) Synergetic material and structural optimization yields robust spider web anchorages. Small 9:2747–2756